NATIONAL INSTITUTE FOR FUSION SCIENCE

A Study of Non-Ideal Focus Properties of 30° Parallel Plate Energy Analyzers

A. Fujisawa, H. Iguchi and Y. Hamada

RESEARCH REPORT
NIFS Series

NAGOYA, JAPAN

A Study of Non-Ideal Focus Properties
of 30° Parallel Plate Energy Analyzers

A. Fujisawa, H. Iguchi, Y. Hamada

National Institute for Fusion Science
464-01, Furo-cho, Chikusa-ku, Nagoya, Japan

Abstract

A succinct model is proposed to describe non-ideal characteristics owing to electric field penetration into the drift region in actual parallel plate energy analyzers. A good agreement has been obtained between the theoretically expected and experimentally observed focus properties of the 30° parallel plate analyzer.

I. Introduction

The 30° parallel plate energy analyzer[1,2] has been used in many fields of science and technology due to its simplicity of the concept and the structure. In the plasma diagnostics, it has been traditionally utilized as the secondary beam energy analyzer of heavy ion beam probes(HIBP) since its second order focusing property is indispensable to minimize the error caused by the difference of the probing beam incident angle[3-6].

Although the parallel transformation symmetry of the parallel plate analyzer allows to predict the approximate characteristics with a simple calculation, the experimentally observed characteristics have been reported to be deviated from the ideal one. This may be ascribed to the incompleteness of the electric field between the parallel plates of the analyzer. In this article, we present a model to describe the focusing properties of the actual energy analyzer on the base of the beam trajectory modification caused by the electric field penetration[7] into the drift region, and compare it with the result of calibration of the 30° parallel plate energy analyzer which has been constructed as a part of a 200keV heavy ion beam probe (HIBP) on the Compact Helical System(CHS).

II. Brief Review of Parallel Plate Analyzer Theory

The parallel plate energy analyzer, whose schematic view is shown in Fig. 1, consists of the drift and the uniform electric field regions. The beam energy is determined by measuring the horizontal range of the beam from the entrance slit to the detector position. The range is also dependent, however,

on the analyzer voltage and the beam incident angle. The dependence of the range on the beam incident angle should be as weak as possible for accurate measurements of beam energy.

The horizontal distance L between the entrance slit and the detector in Fig. 1 is expressed as

$$L = \frac{\alpha_0}{\tan\theta} + \beta_0 \sin 2\theta \ , \tag{1}$$

$$\alpha_0 = h_1 + h_2 \ , \tag{2}$$

$$\beta_0 = \frac{2V_A}{qV_p}d = \frac{2}{q}Gd \ , \tag{3}$$

where d, V_p and V_A are the distance between the parallel plates, the top plate voltage and the accelerator voltage, respectively, and the parameter $G(= V_A/V_p)$ is called as gain factor. The first and the second terms in Eq. (1) represent to the ranges in the drift and the electric field regions, respectively.

Under the condition that the geometrical parameter α_0 is constant, slight changes of the gain ΔG and the beam incident angle $\Delta\theta$ produce the horizontal displacement ΔL represented as

$$\Delta L(\Delta\theta, \ \Delta G) = \Delta L(\Delta\theta) + \Delta L(\Delta G) \ , \tag{4}$$

where the explicit form of the second term is

$$\Delta L(\Delta G) = \frac{2}{q}\Delta G d \sin 2\theta \ . \tag{5}$$

As for the first term, to minimize the beam incident angle dependence, the following condition is imposed on the geometrical parameters of the analyzer;

$$\frac{\partial L}{\partial\theta} = -\frac{\alpha_0}{\sin^2\theta_0} + 2\beta_0 \cos 2\theta_0 = 0 \ , \tag{6}$$

where θ_0 is the standard beam incident angle. Then the second and third order differential coefficients are

$$\frac{\partial^2 L}{\partial \theta^2} = \frac{2\cos\theta_0}{\sin^3\theta_0}\alpha_0 - 4\beta_0\sin 2\theta_0 = \frac{4\beta_0\cos 3\theta_0}{\sin\theta_0} \ , \tag{7}$$

$$\frac{\partial^3 L}{\partial \theta^3} = -\frac{2(1+2\cos^2\theta_0)}{\sin^4\theta_0}\alpha_0 - 8\beta_0\cos 2\theta_0 = -\frac{12\beta_0\cos 2\theta_0}{\sin^2\theta_0} \ , \tag{8}$$

respectively. In the form of the Taylor expansion, the displacement is given by

$$\Delta L(\Delta\theta) = \frac{2\beta_0\cos 3\theta_0}{\sin\theta_0}\Delta\theta^2 - \frac{2\beta_0\cos 2\theta_0}{\sin^2\theta_0}\Delta\theta^3 + \cdots \ . \tag{9}$$

The condition of $\partial L/\partial\theta = \partial^2 L/\partial\theta^2 = 0$ is realized when $\beta_0 = 4\alpha_0$, $\theta_0 = 30°$. The 30° parallel plate energy analyzer, therefore, owns the desirable focusing property of beam injection angle and a wide acceptance angle. It follows that uncertainty in the beam incident angle gives a minimum error to accurate beam energy measurements.

III. Experimental Derivation of Beam Incident Angle Dependence of 30° Parallel Plate Analyzer

A. Split Plate Detector

The split plate detector in Fig. 1b has been used for the energy analyzer of heavy ion beam probes since the detector has a sufficient sensitivity to a small beam displacement. The beam displacement on the split plate detector is measured as the difference between the beam currents of the top and the ground plates. If the beam current profile is uniform, the detected current

difference is related to the displacement Δx as

$$\xi = \frac{i_T - i_B}{i_T + i_B} = \frac{2\Delta x}{w} = \frac{2\Delta L \sin \theta}{w} , \tag{10}$$

where i_T, i_B and w are the currents on the top, the ground plates, respectively, the entrance slit width, and ξ is called here as the beam displacement parameter. Corresponding to Eq. (4), the beam displacement parameter is divided into two parts;

$$\begin{aligned}
\xi(\Delta\theta, \ \Delta G) &= \xi(\Delta\theta) + \xi(\Delta G) \\
&= \frac{2\Delta L(\Delta\theta)\sin\theta}{w} + \frac{2\Delta L(\Delta G)\sin\theta}{w} .
\end{aligned} \tag{11}$$

B. 30° Parallel Plate Energy Analyzer for CHS HIBP

A 30° parallel plate energy analyzer has been constructed for a 200keV heavy ion beam probe on the Compact Helical System(CHS). The energy analyzer's geometrical parameters in Fig. 1 are $d = 75$mm, $h_1 = h_2 = 5d/8 = 46.9$mm, and the gain factor is designed to be 5 for secondary beams ($q = 2$), hence $\beta_0 = 5$. Figure 3 illustrates the top and the ground plates; the ground plate has the beam entrance and exit holes, and the top plate also has a larger hole to make UV light from the plasma go through to avoid voltage break down. Wires of 0.1mm diameter are strained every 5mm on these holes in order to diminish the electric field penetration into the field free regions.

Before installing the analyzer on the CHS, the analyzer's property was examined using a Li$^+$ beam. The split plate detector of the analyzer is

movable along the line AA' in Fig. 1a to be adjusted at the exact focus point. In order to adjust the beam entrance angle, the energy analyzer has a mechanism to rotate itself around the entrance slit to θ-direction. This system permits us to investigate the dependence of the beam displacement parameter on the beam incident angle $\xi(\Delta\theta)$.

When the Li^+ beam is accelerated to 10.000keV, the necessary analyzer voltage to obtain $\xi = 0$ is 4.112keV within a precision of our voltage measurement. Thus, the actual gain is 4.864 for secondary beam ($q = 2$), which is 2.7% smaller than the designed value of 5.0. Figure 3 indicates the experimental angle dependencies of $\xi(\Delta\theta)$ for three different detector positions. When $h_2 = 52.0$mm, the dependence has a flat region around $\Delta\theta = 0$, which is consistent with that it has no zero component proportional to $\Delta\theta$ in the Taylor series. This means that the focus point is extended by $\Delta\alpha = \alpha - \alpha_0 = 5.1$mm. The open squares and circles in Fig. 3 indicate the dependencies when the detector is located around focus by about $\varepsilon = 0.1 \sim 0.2$ mm, $-0.1 \sim -0.2$mm, respectively. The displacement of the detector by $\varepsilon/\alpha_0 = 1.7 \sim 3.3\%$ gives a significant change of the focus property, thus, the detector location should be carefully determined.

IV. Model of Non-Ideal Parallel Plate Energy Analyzer

A. Modified Trajectory Model

In an actual parallel plate analyzer, a clear boundary does not exit between the drift and the electric field regions. The electric field should pen-

etrate into the drift region and should not be completely uniform between the plates. After the beam passes through the entrance aperture, the beam should suffer a small downward acceleration in the drift space due to the leakage field which becomes stronger as closer to the boundary, and it results in the gradual beam deflection in the drift space.

In our model, it is assumed that the deflection should occur at the boundaries between the drift and the electric field regions, and that the beam should experience the same amount of deflection in the entrance and exit boundaries. Then, the modified trajectory is written as

$$L = \frac{\alpha}{\tan \theta} + \beta \sin 2(\theta + \delta\theta) , \tag{12}$$

where $\delta\theta$ is the deflection angle which should have a small negative value. Owing to the field penetration, the electric field generated between the parallel plates should be weaker than the ideal value of $E(= V_{\mathrm{p}}/d)$. By introducing another parameter d_{eff} to describe this effect, the net electric field is expressed as $E_{\mathrm{eff}} = V_{\mathrm{p}}/d_{\mathrm{eff}}$. The parameter β is reformed into

$$\beta = \frac{2}{q} G_{\mathrm{mod}} d_{\mathrm{eff}} , \tag{13}$$

where G_{mod} is the modified gain factor.

In the modified trajectory theory the focusing condition of first order is

$$\frac{\partial L}{\partial \theta} = -\frac{\alpha}{\sin^2 \theta_0} + 2\beta \cos 2(\theta_0 + \delta\theta) = 0 . \tag{14}$$

Since the detector is restricted on the line AA' in Fig. 1, the horizontal range of the beam in the electric field region should be the same as that of the ideal case, hence,

$$\beta \sin 2(\theta_0 + \delta\theta) = \beta_0 \sin 2\theta_0 . \tag{15}$$

It follows from Eqs. (14, 15) that the geometrical parameters α and β are obtained as

$$\alpha = \frac{2\beta_0 \sin^2 \theta_0 \sin 2\theta_0 \cos 2(\theta_0 + \delta\theta)}{\sin 2(\theta_0 + \delta\theta)} \tag{16}$$

$$\beta = \frac{\beta_0 \sin 2\theta_0}{\sin 2(\theta_0 + \delta\theta)} \cdot \tag{17}$$

Since a negative deflection angle ($\delta\theta < 0$) gives a longer α than α_0, the beam deflection should cause an extension of focus length. Insertion of our analyzer's experimental values of $G_0 = 4.864$, $\alpha = 52.0$mm into Eqs. (16, 17) yields the parameters $\delta\theta = -0.67°$, $d_{\text{eff}} = 78.2$; $d_{\text{eff}}/d = 1.042$. The electric field is actually 4.2% weaker than the ideal value.

This modified trajectory theory can predict the beam displacement parameter as a function of the beam incident angle, and here we generalize it to the case with the detector located out of focus. Assuming $\alpha = \alpha_0 + \delta\alpha + \varepsilon$, where $\delta\alpha$, ε are the distance of focus point from the ideal one, the distance from the focus point, respectively, the differential coefficients are given by

$$\frac{\partial L}{\partial \theta} = -\frac{\varepsilon}{\sin^2 \theta_0} , \tag{18}$$

$$\frac{\partial^2 L}{\partial \theta^2} = \frac{4\beta \cos 3\theta_0}{\sin \theta_0} + \frac{2 \cos \theta_0}{\sin^3 \theta_0}(\delta\alpha + \varepsilon) , \tag{19}$$

$$\frac{\partial^3 L}{\partial \theta^3} = -\frac{6\alpha}{\sin^4 \theta_0} , \tag{20}$$

where in the reduction we utilize the relation of Eqs. (14,15). Thus, the horizontal displacement is

$$\Delta L(\Delta\theta) = \frac{\varepsilon}{\sin^2 \theta_0}\Delta\theta - \left(\frac{2\beta \cos 3\theta_0}{\sin \theta_0} + \frac{\cos \theta_0}{\sin^3 \theta_0}(\delta\alpha + \varepsilon)\right)\Delta\theta^2 + \frac{\alpha}{\sin^4 \theta_0}\Delta\theta^3 + \cdots . \tag{21}$$

When $\Delta\theta_0 = 30°$, the above formula gives

$$\Delta L(\Delta\theta) = 4\varepsilon\Delta\theta - 4\sqrt{3}(\delta\alpha + \varepsilon)\Delta\theta^2 + 16\alpha\Delta\theta^3 + \cdots. \qquad (22)$$

Thus, a finite extension of the focus length should break the second order focusing condition which will be achieved in the ideal 30° parallel plate analyzer.

B. Comparison with Experimental Results

Using Eqs. (10, 21), the present model deduces the dependence of the displacement parameter on the beam incident angle as

$$\xi(\Delta\theta) = \frac{2\sin\theta}{w}\left\{\frac{\varepsilon}{\sin^2\theta_0}\Delta\theta - \left(\frac{2\beta\cos 3\theta_0}{\sin\theta_0} + \frac{\cos\theta_0}{\sin^3\theta_0}(\delta\alpha + \varepsilon)\right)\Delta\theta^2\right.$$
$$\left. +\frac{\alpha}{\sin^4\theta_0}\Delta\theta^3 + \cdots\right\}, \qquad (23)$$

where $\theta = \theta_0 + \Delta\theta$. Figure 4 shows the experimentally obtained angle dependence of $\xi_{exp}(\Delta\theta)$, and the theoretical ones expected from the ideal $\xi_{ideal}(\Delta\theta)$ and the modified theory $\xi_{mod}(\Delta\theta)$. The ideal and modified dependencies in the form of polynomial expansion are

$$\xi_{ideal}(\Delta\theta) = -1500\Delta\theta^3 + \cdots, \qquad (24)$$

$$\xi_{mod}(\Delta\theta) = 36\Delta\theta^2 - 1521\Delta\theta^3 + \cdots, \qquad (25)$$

respectively, where $q = 2$ and the slit width of our analyzer $w =$1mm are substituted. On the other hand, using the least square fitting method the experimental angle dependence is expressed as

$$\xi_{exp}(\Delta\theta) = 25\Delta\theta^2 - 1522\Delta\theta^3 + \cdots. \qquad (26)$$

The predicted dependence, therefore, is quantitatively closer to the experimental result than the ideal one. It should be notified that the relative value of the beam incident angle is measured to an accuracy of 0.04°, however, the angle of $\theta_0 = 30°$ is determined with an uncertainty of less than $0.25°(\sim 0.004\text{rad})$. Figure 5 demonstrates the comparison of the dependencies predicted from our model with the experimental ones when the detector is located out of focus. In deriving the theoretical curves we assume $\varepsilon/d = \pm0.15/75$ since the detector position was not measured in sufficient precision. However, a qualitative agreement can be seen in the behavior of the curves.

C. Gain Curve Derivation

For the practical use, the acceptance angle window is characterized by the gain curve whose definition is to satisfy $\Delta L = \Delta L(\Delta\theta) + \Delta L(\Delta G) = 0$. By substituting $\theta_0 = 30°$, the combination of Eqs. (5-9) yields the explicit form of the ideal gain curve as

$$G_{\text{ideal}}(\Delta\theta) = G_{\text{ideal}}(0) - \frac{q\Delta L_{\Delta\theta}}{2d\sin 2\theta} \tag{27}$$

$$= G_{\text{ideal}}(0) + \frac{q}{\sqrt{3}d}(20\Delta\theta^3 + \cdots) . \tag{28}$$

The flat region of this curve can be recognized as the acceptance angle window of the analyzer. On the other hand, since in our model the horizontal displacement due to the change of gain is

$$\Delta L(\Delta G) = \frac{2}{q}\Delta G d_{\text{eff}} \sin 2(\theta + \Delta\theta) , \tag{29}$$

the gain curve at $\theta_0 = 30°$ is written as

$$G_{\text{mod}}(\Delta\theta) = G_{\text{mod}}(0) + \frac{q}{d_{\text{eff}} \sin 2(\theta + \delta\theta)} \left(-4\sqrt{3}\delta\alpha\Delta\theta^2 + (20 + 16\delta\alpha)\Delta\theta^3 + \cdots\right) ,$$

$$(30)$$

where $\theta = \theta_0 + \Delta\theta$, and $\varepsilon = 0$ is assumed. Compared with the ideal case, a finite second coefficient of $\Delta\theta^2$ owing to an extension of the focus makes the acceptance angle window narrower.

The gain curves based on the ideal and our model can be related to the displacement parameter $\xi(\Delta\theta)$ as

$$G_{\text{mod}}(\Delta\theta) = G_{\text{mod}}(0) - \frac{qw\xi(\Delta\theta)}{4d_{\text{eff}} \sin 2(\theta + \delta\theta) \sin\theta} , \qquad (31)$$

$$G_{\text{ideal}}(\Delta\theta) = G_{\text{ideal}}(0) - \frac{qw\xi(\Delta\theta)}{4d \sin 2\theta \sin\theta} , \qquad (32)$$

respectively. Figure 6 shows the gain curves calculated with the above formulae. The theoretical curves are derived with the condition of $G_{\text{ideal}}(0) = G_{\text{mod}}(0) = 4.864$. Note that the gain curves are calibrated for the secondary ion beams ($q = 2$) for the heavy ion beam probe application. Both experimentally derived curves do not have so much difference, while the modified gain curve has, as similar to the case of the displacement parameter, a good agreement with the experimental ones.

V. Concluding Remarks

The present model can describe successfully the experimental focus properties of the 30° parallel plate energy analyzer. The extension of the focus length and the deviation of the focus properties from the ideal one should be ascribed to the beam deflection near the boundaries between the electric

field and the field-free drift regions. A more complicated computer simulation of the beam trajectories in the electric field calculated with the boundary element or the finite element methods will also give a possible and more complete explanation to the displacement of the focus position and the non-ideal characteristics of the angle dependencies. However, our simple treatment is sufficient to interpret the experimental results, and the conciseness of the model is suitable for a practical use.

References

1) T. S. Green and G. A. Proca, Rev. Sci. Instrum. 41, 1409(1970).

2) G. A. Proca and T. S. Green, Rev. Sci. Instrum. 41, 1778 (1970).

3) L. Solensten and K. A. Connor, Rev. Sci. Instrum. 58, 516(1987).

4) S. C. Aceto, K. A. Connor, P. E. McClaren, J. J. Zielinski, and J. G. Schatz, Rev. Sci. Instrum. 61, 2958(1990).

5) P. E. McClaren, K. A. Connor, J. F. Lewis, R. L. Hickok, T. P. Crowley, J. G. Schatz and G. H. Vilardi, Rev. Sci. Instrum. 61, 2955(1990).

6) Y. Hamada, Y. Kawasumi, K. Masai, H. Iguchi, A. Fujisawa, Y. Abe, Rev. Sci. Instrum. 63, 4446(1992).

7) J. J. Zielinski, Private Communication.

Figure Captions

Fig.1: (a)Schematic view of the Proca and Green type analyzer. (b)Split Plate detector.

Fig.2: Top and ground plates of the 30° parallel plate energy analyzer for CHS HIBP. The length is measured in the unit of mm.
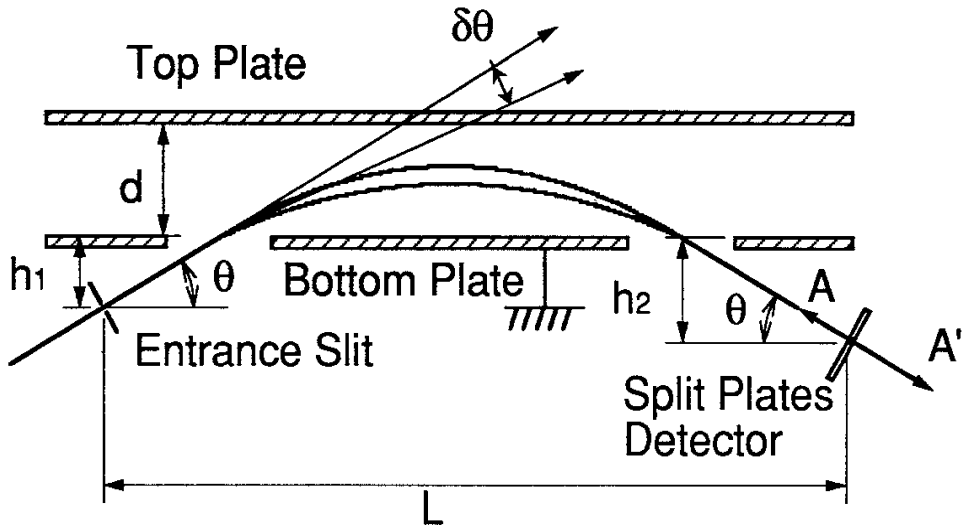
Fig.3: Experimentally obtained focus property of the 30° parallel plate energy analyzer. The close circles represent the beam displacement parameter ξ as a function of the beam incident angle $\Delta\theta$ when the detector is located at the focus point, and the open squares and circles represent the ones when the detector is located around focus by about $\varepsilon = 0.1 \sim 0.2$ mm, $-0.1 \sim -0.2$mm, respectively.

Fig.4: Comparison of the experimental dependence of the beam displacement parameter on the beam incident angle $\xi(\Delta\theta)$ with the ones predicted from the ideal and the presented models. The open circles mean the experimental values.

Fig.5: Comparison of the experimental focus properties with modified ones when the detector is located out of focus. The open and close circles represent the ones when the detector is located around focus by about $\varepsilon = 0.1 \sim 0.2$ mm, $-0.1 \sim -0.2$mm, respectively. In the theoretical curves $\varepsilon/d = \pm 0.15/75$ is assumed.

Fig.6: Experimentally derived gain curves and theoretical ones based on the ideal and the modified theory.
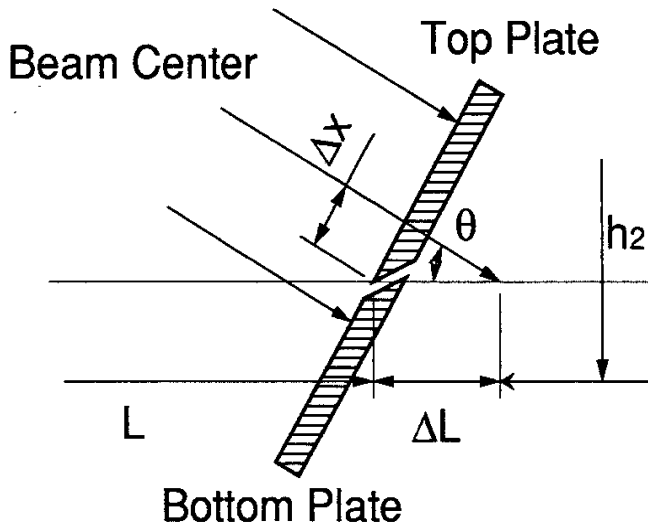
a) Parallel Plate Energy Analyzer

Top Plate

$\delta\theta$

d

h_1

θ

Bottom Plate

h_2

θ

A

A'

Entrance Slit

Split Plates
Detector

L

b) Split Plates Detector

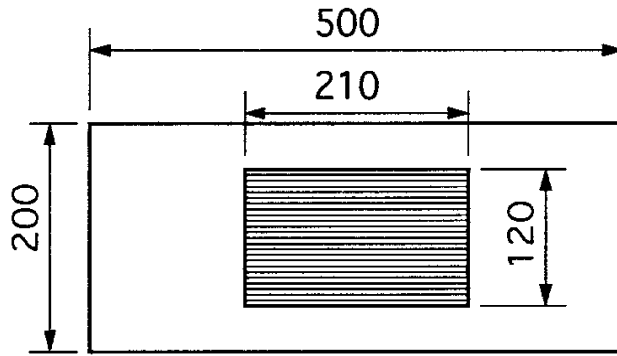Beam Center

Top Plate
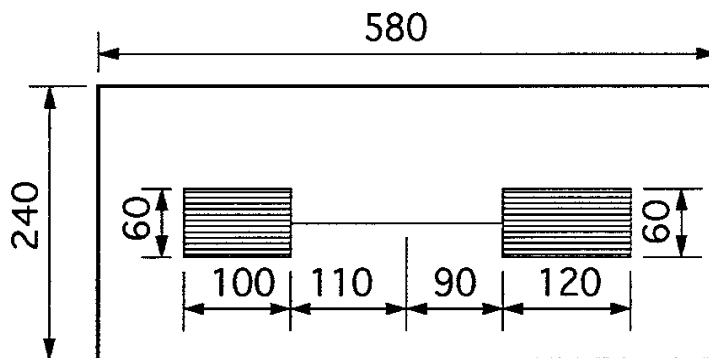
Δx

θ

h_2

L
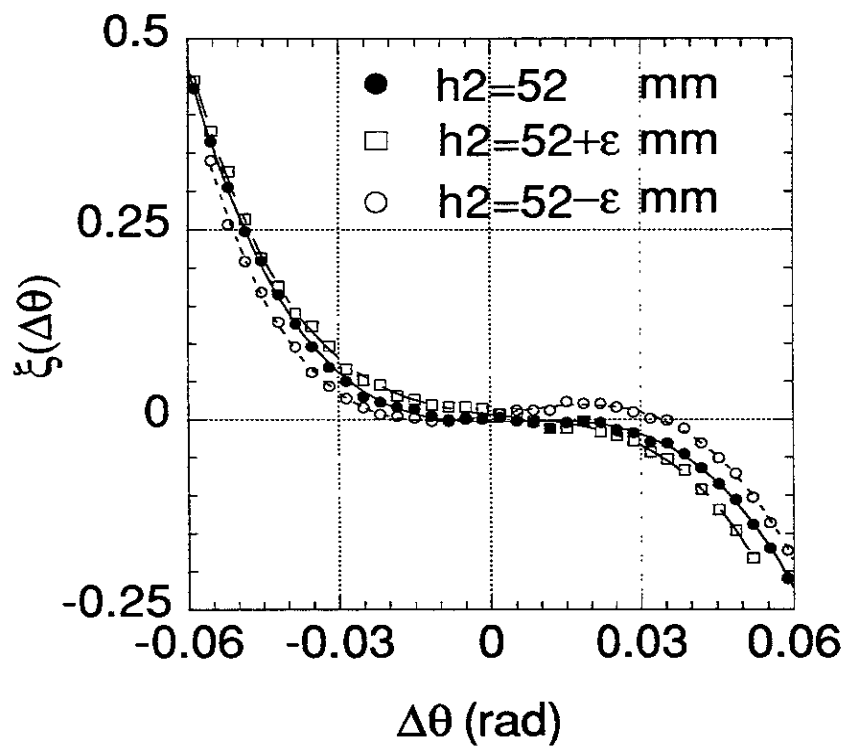
ΔL

Bottom Plate

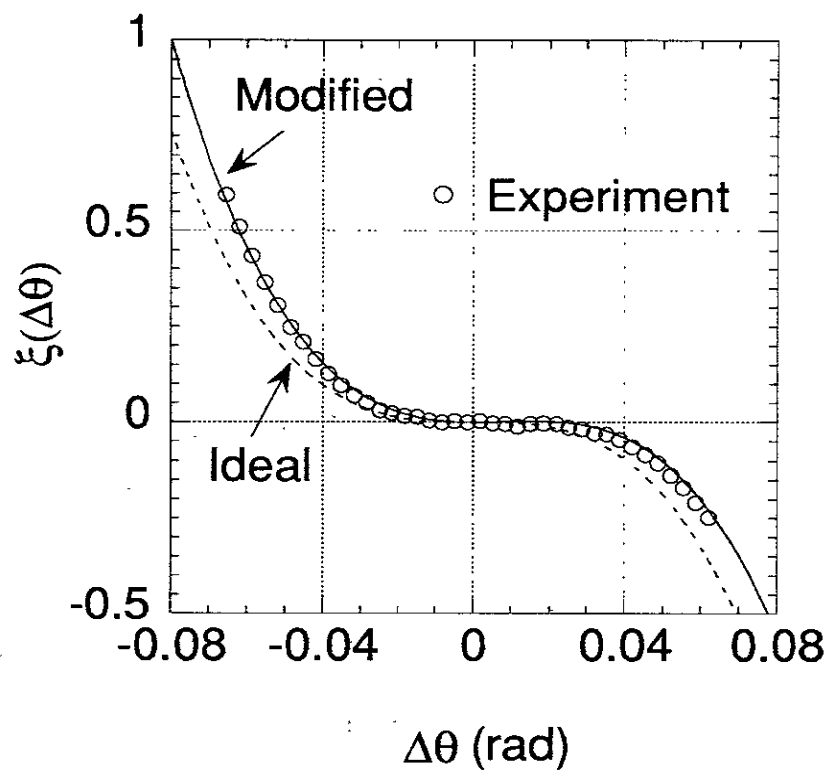Fig. 1

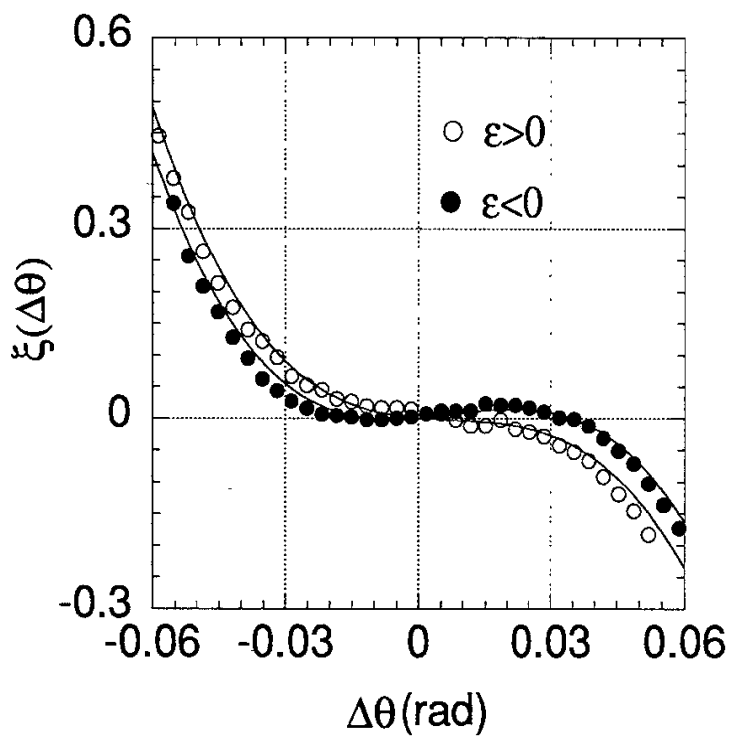# Top Plate

Bottom Plate

Fig. 2

Fig. 3

Fig. 4

Fig. 5
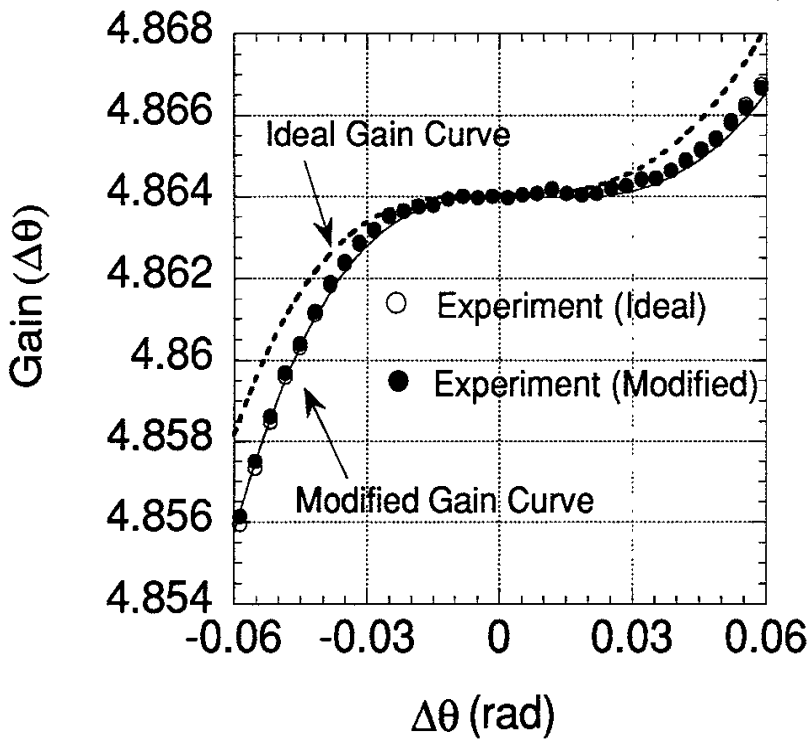
Fig. 6

Recent Issues of NIFS Series

NIFS-213   K. Itoh, H. Sanuki and S.-I. Itoh, *Thermal and Electric Oscillation Driven by Orbit Loss in Helical Systems*; Mar. 1993

NIFS-214   T. Yamagishi, *Effect of Continuous Eigenvalue Spectrum on Plasma Transport in Toroidal Systems*; Mar. 1993

NIFS-215   K. Ida, K. Itoh, S.-I.Itoh, Y. Miura, JFT-2M Group and A. Fukuyama, *Thickness of the Layer of Strong Radial Electric Field in JFT-2M H-mode Plasmas*; Apr. 1993

NIFS-216   M. Yagi, K. Itoh, S.-I. Itoh, A. Fukuyama and M. Azumi, *Analysis of Current Diffusive Ballooning Mode*; Apr. 1993

NIFS-217   J. Guasp, K. Yamazaki and O. Motojima, *Particle Orbit Analysis for LHD Helical Axis Configurations* ; Apr. 1993

NIFS-218   T. Yabe, T. Ito and M. Okazaki, *Holography Machine HORN-1 for Computer-aided Retrieve of Virtual Three-dimensional Image* ; Apr. 1993

NIFS-219   K. Itoh, S.-I. Itoh, A. Fukuyama, M. Yagi and M. Azumi, *Self-sustained Turbulence and L-Mode Confinement in Toroidal Plasmas* ; Apr. 1993

NIFS-220   T. Watari, R. Kumazawa, T. Mutoh, T. Seki, K. Nishimura and F. Shimpo, *Applications of Non-resonant RF Forces to Improvement of Tokamak Reactor Performances Part I: Application of Ponderomotive Force* ; May 1993

NIFS-221   S.-I. Itoh, K. Itoh, and A. Fukuyama, *ELMy-H mode as Limit Cycle and Transient Responses of H-modes in Tokamaks* ; May 1993

NIFS-222   H. Hojo, M. Inutake, M. Ichimura, R. Katsumata and T. Watanabe, *Interchange Stability Criteria for Anisotropic Central-Cell Plasmas in the Tandem Mirror GAMMA 10* ; May 1993

NIFS-223   K. Itoh, S.-I. Itoh, M. Yagi, A. Fukuyama and M. Azumi, *Theory of Pseudo-Classical Confinement and Transmutation to L-Mode;* May 1993

NIFS-224   M. Tanaka, *HIDENEK: An Implicit Particle Simulation of Kinetic-MHD Phenomena in Three-Dimensional Plasmas;* May 1993

NIFS-225   H. Hojo and T. Hatori, *Bounce Resonance Heating and Transport in a Magnetic Mirror;* May 1993

NIFS-226   S.-I. Iton, K. Itoh, A. Fukuyama, M. Yagi, *Theory of Anomalous Transport in H-Mode Plasmas;* May 1993

NIFS-227   T. Yamagishi, *Anomalous Cross Field Flux in CHS ;* May 1993

NIFS-228   Y. Ohkouchi, S. Sasaki, S. Takamura, T. Kato, *Effective Emission and Ionization Rate Coefficients of Atomic Carbons in Plasmas;* June 1993

NIFS-229   K. Itoh, M. Yagi, A. Fukuyama, S.-I. Itoh and M. Azumi, *Comment on 'A Mean Field Ohm's Law for Collisionless Plasmas;* June 1993

NIFS-230   H. Idei, K. Ida, H. Sanuki, H. Yamada, H. Iguchi, S. Kubo, R. Akiyama, H. Arimoto, M. Fujiwara, M. Hosokawa, K. Matsuoka, S. Morita, K. Nishimura, K. Ohkubo, S. Okamura, S. Sakakibara, C. Takahashi, Y. Takita, K. Tsumori and I. Yamada, *Transition of Radial Electric Field by Electron Cyclotron Heating in Stellarator Plasmas;* June 1993

NIFS-231   H.J. Gardner and K. Ichiguchi, *Free-Boundary Equilibrium Studies for the Large Helical Device,* June 1993

NIFS-232   K. Itoh, S.-I. Itoh, A. Fukuyama, H. Sanuki and M. Yagi, *Confinement Improvement in H-Mode-Like Plasmas in Helical Systems,* June 1993

NIFS-233   R. Horiuchi and T. Sato, *Collisionless Driven Magnetic Reconnection,* June 1993

NIFS-234   K. Itoh, S.-I. Itoh, A. Fukuyama, M. Yagi and M. *Azumi, Prandtl Number of Toroidal Plasmas;* June 1993

NIFS-235   S. Kawata, S. Kato and S. Kiyokawa , *Screening Constants for Plasma;* June 1993

NIFS-236   A. Fujisawa and Y. Hamada, *Theoretical Study of Cylindrical Energy Analyzers for MeV Range Heavy Ion Beam Probes;* July 1993

NIFS-237   N. Ohyabu, A. Sagara, T. Ono, T. Kawamura and O. Motojima, *Carbon Sheet Pumping;* July 1993

NIFS-238   K. Watanabe, T. Sato and Y. Nakayama, *Q-profile Flattening due to Nonlinear Development of Resistive Kink Mode and Ensuing Fast Crash in Sawtooth Oscillations;* July 1993

NIFS-239   N. Ohyabu, T. Watanabe, Hantao Ji, H. Akao, T. Ono, T. Kawamura, K. Yamazaki, K. Akaishi, N. Inoue, A. Komori, Y. Kubota, N. Noda, A. Sagara, H. Suzuki, O. Motojima, M. Fujiwara, A. Iiyoshi, *LHD Helical Divertor;* July 1993

NIFS-240   Y. Miura, F. Okano, N. Suzuki, M. Mori, K. Hoshino, H. Maeda,
            T. Takizuka, JFT-2M Group, K. Itoh and S.-I. Itoh, *Ion Heat Pulse
            after Sawtooth Crash in the JFT-2M Tokamak;* Aug. 1993

NIFS-241   K. Ida, Y.Miura, T. Matsuda, K. Itoh and JFT-2M Group, *Observation
            of non Diffusive Term of Toroidal Momentum Transport in the JFT-
            2M Tokamak;* Aug. 1993

NIFS-242   O.J.W.F. Kardaun, S.-I. Itoh, K. Itoh and J.W.P.F. Kardaun,
            *Discriminant Analysis to Predict the Occurrence of ELMS in H-
            Mode Discharges;* Aug. 1993

NIFS-243   K. Itoh, S.-I. Itoh, A. Fukuyama,
            Modelling of Transport Phenomena; Sep. 1993

NIFS-244   J. Todoroki,
            Averaged Resistive MHD Equations; Sep. 1993

NIFS-245   M. Tanaka,
            The Origin of Collisionless Dissipation in Magnetic Reconnection;
            Sep. 1993

NIFS-246   M. Yagi, K. Itoh, S.-I. Itoh, A. Fukuyama and M. Azumi,
            *Current Diffusive Ballooning Mode in Seecond Stability Region of
            Tokamaks;* Sep. 1993

NIFS-247   T. Yamagishi,
            *Trapped Electron Instabilities due to Electron Temperature Gradient
            and Anomalous Transport;* Oct. 1993

NIFS-248   Y. Kondoh,
            Attractors of Dissipative Structure in Three Disspative Fluids; Oct.
            1993

NIFS-249   S. Murakami, M. Okamoto, N. Nakajima, M. Ohnishi, H. Okada,
            *Monte Carlo Simulation Study of the ICRF Minority Heating in the
            Large Helical Device;* Oct. 1993

NIFS-250   A. Iiyoshi, H. Momota, O. Motojima, M. Okamoto, S. Sudo, Y. Tomita,
            S. Yamaguchi, M. Ohnishi, M. Onozuka, C. Uenosono,
            Innovative Energy Production in Fusion Reactors; Oct. 1993

NIFS-251   H. Momota, O. Motojima, M. Okamoto, S. Sudo, Y. Tomita,
            S. Yamaguchi, A. Iiyoshi, M. Onozuka, M. Ohnishi, C. Uenosono,
            Characteristics of D-^{3}He Fueled FRC Reactor: ARTEMIS-L,
            Nov. 1993

NIFS-252   Y. Tomita, L.Y. Shu, H. Momota,

Direct Energy Conversion System for D-^{3}He Fusion, Nov. 1993

NIFS-253   S. Sudo, Y. Tomita, S. Yamaguchi, A. Iiyoshi, H. Momota, O. Motojima, M. Okamoto, M. Ohnishi, M. Onozuka, C. Uenosono, *Hydrogen Production in Fusion Reactors,* Nov. 1993

NIFS-254   S. Yamaguchi, A. Iiyoshi, O. Motojima, M. Okamoto, S. Sudo, M. Ohnishi, M. Onozuka, C. Uenosono, *Direct Energy Conversion of Radiation Energy in Fusion Reactor,* Nov. 1993

NIFS-255   S. Sudo, M. Kanno, H. Kaneko, S. Saka, T. Shirai, T. Baba, *Proposed High Speed Pellet Injection System "HIPEL" for Large Helical Device* Nov. 1993

NIFS-256   S. Yamada, H. Chikaraishi, S. Tanahashi, T. Mito, K. Takahata, N. Yanagi, M. Sakamoto, A. Nishimura, O. Motojima, J. Yamamoto, Y. Yonenaga, R. Watanabe, *Improvement of a High Current DC Power Supply System for Testing the Large Scaled Superconducting Cables and Magnets;* Nov. 1993

NIFS-257   S. Sasaki, Y. Uesugi, S. Takamura, H. Sanuki, K. Kadota, *Temporal Behavior of the Electron Density Profile During Limiter Biasing in the HYBTOK-II Tokamak;* Nov. 1993

NIFS-258   K. Yamazaki, H. Kaneko, S. Yamaguchi, K.Y. Watanabe, Y.Taniguchi, O.Motojima, LHD Group, *Design of Central Control System for Large Helical Device (LHD);* Nov. 1993

NIFS-259   K. Yamazaki, H. Kaneko, S. Yamaguchi, K.Y. Watanabe, Y.Taniguchi, O.Motojima, LHD Group, *Design of Central Control System for Large Helical Device (LHD);* Nov. 1993

NIFS-260   B.V.Kuteev, *Pellet Ablation in Large Helical Device;* Nov. 1993

NIFS-261   K. Yamazaki, *Proposal of "MODULAR HELIOTRON': Advanced Modular Helical System Compatible with Closed Helical Divertor;* Nov. 1993

NIFS-262   V.D.Pustovitov, *Some Theoretical Problems of Magnetic Diagnostics in Tokamaks and Stellarators;* Dec. 1993